RSC Advances

PAPER

Cite this: *RSC Adv.*, 2018, **8**, 23981

$Eu^{3+/2+}$ co-doping system induced by adjusting Al/Y ratio in Eu doped $CaYAlO_4$: preparation, bond energy, site preference and $^5D_0-^7F_4$ transition intensity†

Yu Pan,[a] Wenjun Wang,[a] Yuhan Zhu,[a] Haibing Xu,[a] Liqun Zhou,[a] Hyeon Mi Noh,[b] Jung Hyun Jeong,*[b] Xiaoguang Liu*[a] and Ling Li*[a]

Received 24th May 2018
Accepted 25th June 2018

DOI: 10.1039/c8ra04432e

rsc.li/rsc-advances

$CaY_{1-x}Al_{1+x}O_4$:2%Eu ($x = 0$, 0.1, 0.2) phosphors have been synthesized *via* a solid-state reaction process. XRD patterns indicate that they are pure phase. The photoluminescence properties of the $CaY_{1-x}Al_{1+x}O_4$:2%Eu phosphors exhibit both the blue emission of Eu^{2+} ($4f^65d^1-4f^7$) and red-orange emission of Eu^{3+} ($^5D_0-^7F_{1,2,3,4}$) under UV light excitation, which showed that the $Eu^{3+/2+}$ co-doping system was obtained by adjusting the Al/Y ratio. Eu^{3+} ions can be reduced to Eu^{2+} ions when the Al/Y ratio was changed. In this work, the bond energy method was used to determine and explain the mechanism of the site occupation of Eu ions entering the host matrix. Also, the emission spectrum showed an unusual comparable intensity $^5D_0-^7F_4$ transition peak. The relative intensity of $^5D_0-^7F_2$ and $^5D_0-^7F_4$ can be stabilized by changing the relative proportions of Al^{3+} and Y^{3+}. Furthermore, this was explained by the J–O theory.

1. Introduction

Rare-earth ions, as widely used activators, have been playing an irreplaceable role in lighting-emitting diodes (LEDs),[1] due to their abundant emission colors based on the 4f–4f or 5d–4f transitions.[2,3] The luminescence properties of different rare earth ions deliver an explicit comprehension on the internal correlations between them, which is generally determined by electronic configuration of the dopant and dynamic coupling between the dopant and the host lattices.[4,5] The local structure around the rare earth in the crystal lattice also plays an important role in controlling its luminescence performance especially the 4f–5d transitions.[6,7]

Eu ions, including Eu^{3+} and Eu^{2+}, are the most commonly used activators in phosphor materials among the rare-earth ions.[8–10] Eu^{2+} ions emit a tunable color ranging from ultraviolet to red due to its 5d–4f transition.[11,12] The 5d orbit of Eu^{2+} is strongly affected by the environment of the crystal, thus the emission of Eu^{2+} is strongly influenced by the crystal field.[13] Eu^{3+} is one of the most frequently used red-emitting activators, which mainly shows characteristic emissions resulting from the transitions of $^5D_0-^7F_J$ ($J = 0$, 1, 2, 3, 4).[14,15] However, the partly-forbidden f–f transitions of Eu^{3+} have low oscillator strength, resulting in low absorption efficiency and a low color rendering index (CRI). Therefore, it is a promising method to overcome the limitations of Eu^{3+} activated phosphors *via* the coexistence of Eu^{3+} and Eu^{2+} in single phase phosphors.[16]

The $Eu^{3+/2+}$ co-doped phosphors can be prepared through a reduction annealing process in a reducing atmosphere such as H_2, H_2/N_2 mixture or CO.[16] After that, the Eu^{3+}/Eu^{2+} co-doped phosphor can be obtained when Eu^{3+} was reduced to Eu^{2+} partially not completely. However, it is very difficult to obtain the Eu^{3+}/Eu^{2+} co-doped $CaYAlO_4$ even through conventional high temperature solid-state reaction under a reducing atmosphere. Another extreme example is Eu ion doped $CaAl_2O_4$, in which an abnormal reduction of $Eu^{3+} \rightarrow Eu^{2+}$ was observed in monoclinic phase of $CaAl_2O_4$: Eu that calcined in air atmosphere at high temperature.[17,18] Comparing the formula of CaYAlO4 and $CaAl_2O_4$, the only change is their Al/Y ratio. Herein, we investigated the $CaY_{1-x}Al_{1+x}O_4$:2%Eu system by adjusting the Al/Y ratio. In our work, the phenomenon of the reduction of Eu^{3+} to Eu^{2+} in $CaY_{1-x}Al_{1+x}O_4$ systems was observed, and the bond energy method is adopted to theoretically explain the site preferential occupancy of Eu^{2+}/Eu^{3+} in the $CaY_{1-x}Al_{1+x}O_4$ systems.

The deviation of its bond energy in different lattice can be compared to determine which site the activators will occupy according to the similar property of chemical bonds and the

[a]*Hubei Collaborative Innovation Center for Advanced Organochemical Materials, Ministry-of-Education Key Laboratory for the Synthesis and Applications of Organic Functional Molecules, Hubei University, Wuhan 430062, China. E-mail: liling402431@hotmail.com; Liuxiaoguang402@hotmail.com*

[b]*Department of Physics, Pukyong National University, Busan 608-737, Korea. E-mail: jhejong@pknu.ac.kr*

† Electronic supplementary information (ESI) available. See DOI: 10.1039/c8ra04432e

similar value of their bond energy.[19] The smaller deviation of the bond energy between the host and activators ions, the more easily the lattice site can be replaced by the ion. Therefore, we use this method to solve the site occupancy problem of doping rare earth ions in the matrix. In the previous research, the site preferential occupancy for Eu in $Sr_2V_2O_7$, $Sr_9Gd(VO_4)_7$ and $Sr_2V_2O_7/Sr_9Gd(VO_4)_7$ phosphors[20] as well as the site occupancy preference of Bi^{2+} in β-$Ca_2P_2O_7$ (ref. 21) crystal have been confirmed though the bond energy method.[19] In addition, the bond energy method can connect the relationship between bond energy and preferential occupancy in Eu^{3+} doped in $CaAl_2Si_2O_8$ crystal.[22] Our calculated results are in good agreement with the experimental data and the photoluminescence spectra.

In addition, Eu^{3+}-doped inorganic phosphors can be used as efficient orange to red emitting phosphors due to the $^5D_0$–^7F_J (J = 0, 1, 2, 3 and 4) transitions. Most of the phosphors show the dominant emission either $^5D_0 \rightarrow {}^7F_1$ (~593 nm) or $^5D_0 \rightarrow {}^7F_2$ (~610 nm) transition of Eu^{3+} ions. The dominated $^5D_0 \rightarrow {}^7F_4$ (~703 nm) transition emission is infrequent. Only some numerable phosphors show that they have stronger intensity of $^5D_0$–$^7F_4$ than $^5D_0$–$^7F_1$, such as $Sr_{0.99}[La_{(1-x)}Eu_x]_{1.01}Zn_{0.99}O_{3.495}$,[23] $LaBO_3$:Eu^{3+},[24] $Na_9[EuW_{10}O_{36}]\cdot 14H_2O$,[25] Na_2CaSiO_4:Eu^{3+},[26] $Ca_2Ga_2SiO_7$:Eu^{3+},[27] $YAsO_4$:Eu.[28] Similarly, this phenomenon has been found in $CaYAlO_4$ with Eu doped. But, the stronger emission of $^5D_0$–$^7F_4$ disappeared when Eu^{3+} and Tb^{3+} were co-doped into $CaYAlO_4$.[29] However, in our work, the relative intensity of $^5D_0$–$^7F_4$ and $^5D_0$–$^7F_2$ can be modified by changing the Al^{3+} and Y^{3+} ions ratios in $CaY_{1-x}Al_{1+x}O_4$ and the Judd–Ofelt theory[30] was applied to calculate the radiative properties of the prepared materials.

2. Experimental section

2.1 Materials and synthesis

A series of $CaY_{1-x}Al_{1+x}O_4$:2%Eu (x = 0, 0.1, 0.2, 0.3, 0.4) phosphors was prepared by a traditional high temperature solid-state reaction route using stoichiometric amounts of $CaCO_3$ (A.R.), Y_2O_3 (99.99%), Al_2O_3 (99.99%), Eu_2O_3 (99.99%) as raw materials, after the reactants were mixed and well-ground in an agate mortar, they were preheated at 1400 °C for 4 hours. Then the mixtures were reground and calcined at 1500 °C for 4 hours. All of $CaY_{1-x}Al_{1+x}O_4$:2%Eu (x = 0, 0.1, 0.2, 0.3, 0.4) phosphors prepared under a reducing atmosphere of H_2 (5%) and N_2 (95%). The final power products were obtained after cooling to room temperature and grinding to powder sample.

2.2 Characterization

The phase purity of the products was examined by X-ray diffraction (XRD) using a BRUKER D8 ADVANCE powder diffractometer with Cu Kα radiation (0.15405 nm) at room temperature, the diffraction data were collected in 2θ range from 5 to 90°. The UV-vis diffuse reflectance spectra were collected through a Cary 5000 UV-vis-NIR spectrophotometer equipped with a double out-of-plane Littrow monochromator using $BaSO_4$ as a standard reference. All excitation, emission, decay spectra and quantum efficiency were measured on an Edinburgh FLS980 combined fluorescence lifetime, a 450 W xenon lamp was used as the excitation source of emission spectra, while a 60 W μF flash lamp with a pulse width of 1.5–3.0 μs was for the measurements of decay curves.

3. Result and discussion

3.1 Phase characterization

For comparison, the $CaYAlO_4$:2%Eu was prepared firstly under a reducing atmosphere of H_2 (5%) and N_2 (95%). The XRD patterns of the $CaYAlO_4$:2%Eu together with the Joint Committee on Powder Diffraction Standards (JCPDS) card no. 24-0221 are shown in Fig. 1(a). The XRD patterns of $CaYAlO_4$:2% Eu shows that the diffraction peaks of all single samples are matched well with the standard card of $CaYAlO_4$ (JCPDS: 24-0221), which indicates that the samples are purity phase and doping Eu ions do not cause significant changes to the crystal structure.

In order to get further confirmation and knowledge regarding crystal structure information and sites of $CaYAlO_4$:2% Eu, the XRD Rietveld refinement of $CaYAlO_4$:2%Eu were performed by the General Structure Analysis System (GASA) program with the single crystallographic data of $CaYAlO_4$ as the initial model. Fig. 1(b) presents red lines and black lines stand for experimental and calculated patterns, respectively, which matched well with each other. The obtained converged weighted-profiles of R_p = 8.4% and R_{wp} = 6.1%, which reveals a good quality of fit. As the crystallographic data of $CaYAlO_4$:2% Eu shown in Table 1. And Fig. S1† shows the XRD refinements of $CaY_{0.9}Al_{1.1}O_4$:2%Eu and $CaY_{0.8}Al_{1.2}O_4$:2%Eu. This aluminate compound has a tetragonal crystal system with space group $I4/mmm$, $a = b = 3.664$ Å, $c = 11.889$ Å, $V = 159.61$ Å^3. However, the lattice constants of $CaYAlO_4$:2%Eu are $a = b = 3.648$ Å, $c = 11.885$ Å, which indicates that its crystal constants increase with increasing the concentration of Eu^{3+}.

$CaYAlO_4$ has a tetragonal K_2NiF_4 structure and belongs to a family of compounds with the general formula $ABCO_4$, where A is an alkaline earth cation, B is Y, Sc, or a trivalent rare earth element and C is Al, Ga or a transition metal ion. In the unit cell, as shown in Fig. 1(c), the Ca and Y cations are distributed almost statistically in the nine coordinated sites and Al^{3+} ions are coordinated with six oxygen atoms and form the AlO_6 octahedron.

Notably, the $(Ca/Y)O_9$ polyhedron is closely surrounded by AlO_6 octahedrons to form a cage structure (Fig. S2†). Thus, it can be concluded that the local environment of Ca/Y sites is highly compressed due to the rigid structure of $CaYAlO_4$, which gives rise to the difficulty of reduction of Eu^{3+} activators. The Lin *et al.* has been reported an effective approach-crystal-site engineering to control Eu^{3+} reduced to Eu^{2+}.[16] So, a similar way has been used to change the reduction of Eu^{3+} doped in $CaYAlO_4$.

Compared with Eu^{3+}, the smaller ions will replace the Al^{3+} site (such B^{3+} and Si^{4+}), therefore, an artificial defect substitution will be used for Al^{3+} doping to $CaYAlO_4$. Fig. 2 showed the XRD patterns of $CaY_{1-x}Al_{1+x}O_4$:2%Eu (x = 0–0.4). Compared with standard card of $CaYAlO_4$, When $x > 0.2$, the XRD pattern diffraction peak appeared a weak miscellaneous

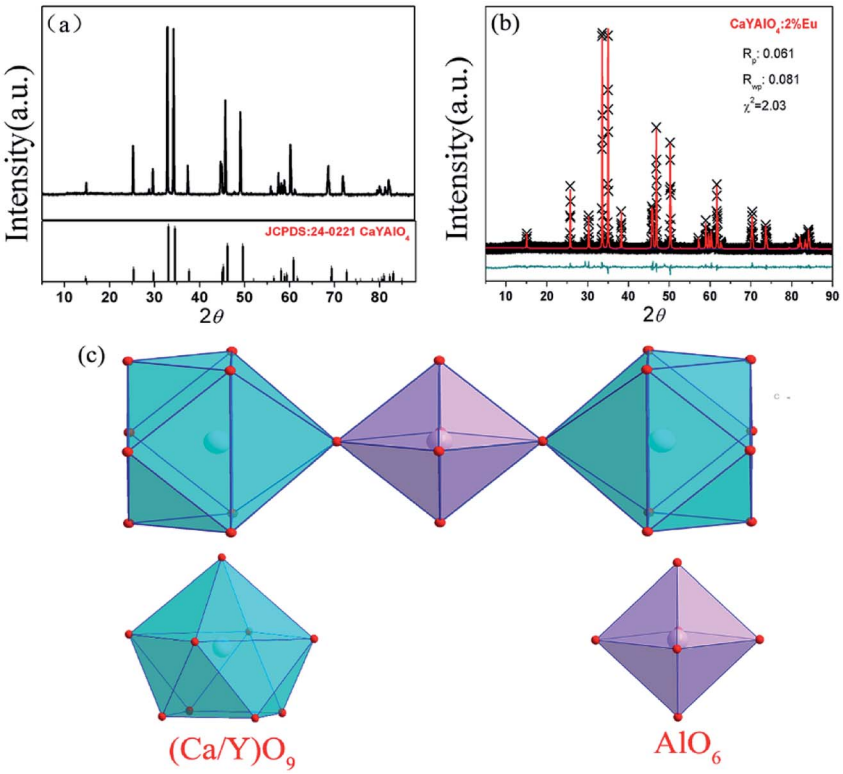

Fig. 1 (a) Powder X-ray diffraction (XRD) patterns of $CaYAlO_4$:2%Eu^{3+} and the standard cards of $CaYAlO_4$ (JCPDS: 24-0221); (b) experimental (cross), calculated (solid line) and difference (bottom) results of XRD refinements of $CaYAlO_4$:2%Eu^{3+}. (c) The crystal structure of $CaYAlO_4$. Ca^{2+}or Y^{3+} ions are coordinated with nine oxygen atoms to form CaO_9 or YO_9 group and Al^{3+} ions are coordinated with six oxygen atoms and form the AlO_6 octahedron.

Table 1 Crystallographic data of $CaYAlO_4$:0.02Eu^{3+}, as determined by the Rietveld refinement of powder XRD data at room temperature

Atom	Site	x	y	z	Occupancy
Ca1	4e	0.0000	0.0000	0.3604	0.500
Y1	4e	0.0000	0.0000	0.3603	0.490
Eu1	4e	0.0000	0.0000	0.5000	0.010
Al1	2a	0.5000	0.5000	0.5000	1.000
O1	4e	0.5000	0.0000	0.5000	1.000
O2	4e	0.0000	0.0000	0.1686	1.000

peak around 31°, which indicates that a new phase appeared at this time, the diffraction peak at about 31 degrees is described to $Ca_3Y_2O_6$, the strongest exact diffraction peak of $CaAl_2O_4$ is at 30 degrees (see Fig. S3†), so the impurity cannot be ascribed to $CaAl_2O_4$. In addition, the properties of luminescence for Eu ions doped in $Ca_3Y_2O_6$ crystals aren't detected in research works at present, which indicates that the Eu^{2+} or Eu^{3+} in $Ca_3Y_2O_6$ has not any emission at room temperature. When $x \leq 0.2$, the diffraction peak of the sample is consistent with the standard card diffraction peak, which means that the Al^{3+} actually occupy the Y^{3+} within a certain range. Thus, we restricted the x value to a maximum of 0.20. Table 2 summarizes the lattice parameters and reliability factors of $CaY_{1-x}Al_{1+x}O_4$:2%Eu. In addition, because the Al^{3+} ion radius is smaller than that of Y^{3+}, the volume of the unit cell will decrease when Al^{3+} occupies the Y^{3+} site.

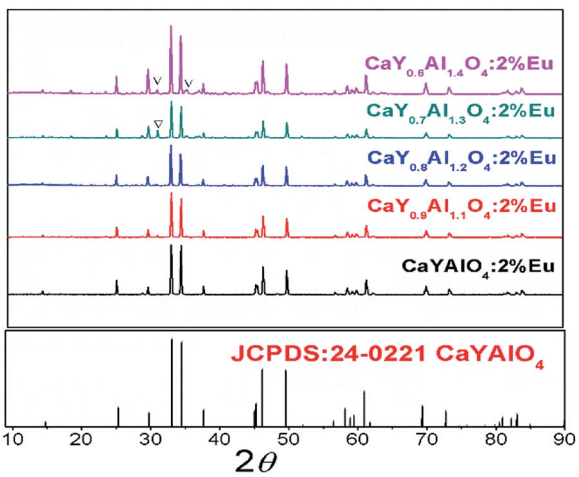

Fig. 2 The powder X-ray diffraction patterns of $CaY_{1-x}Al_{1+x}O_4$:2%Eu (x = 0–0.4) and the standard cards of $CaYAlO_4$ (JCPDS: 24-0221).

3.2 Photoluminescence properties

For Eu doped samples, one can clearly distinguish the different emission bands from the photoluminescence (PL) properties of the two valence states of Eu, *i.e.*, the broad ones are attributed to the parity-allowed 4f–5d transitions of Eu^{2+} and the sharp ones are ascribed to the parity–forbidden transitions of Eu^{3+} ($^5D_0 \rightarrow$

Table 2 The lattice parameters and reliability factors of $CaY_{1-x}Al_{1+x}O_4$:2%Eu ($x = 0$, 0.1, 0.2)

Sample	$CaYAlO_4$	$CaY_{0.9}Al_{1.1}O_4$	$CaY_{0.8}Al_{1.2}O_4$
R_{wp}	0.081	0.092	0.101
R_p	0.061	0.071	0.082
χ^2	2.410	2.030	3.890
$a = b$ (Å)	3.664	3.642	3.610
c (Å)	11.889	11.882	11.859
V (Å^3)	159.61	157.60	154.55

^7F_J, $J = 0$–4). Fig. 3(a), (c) and (f) illustrate the emission spectra of $CaY_{1-x}Al_{1+x}O_4$:2%Eu ($x = 0$, 0.1, 0.2) samples under the NUV excitation of 365 nm. When $x = 0$, as shown in Fig. 3(b), the photoluminescence excitation (PLE) spectrum monitored at 622 nm reveals a broad band with the peak at 277 nm in the range of 200–350 nm due to the charge transfer band (CTB) from O to the Eu ions, along with some sharp peaks in the range of 350–500 nm related to the 4f–4f transitions of Eu^{3+} ions. Under the excitation of 277 or 365 nm, only the sharp f–f transitions can be found. The sharp emission lines of $CaYAlO_4$:Eu can be assigned to f–f transition of Eu^{3+}, which indicates that Eu^{3+} could not be directly reduced to Eu^{2+} in $CaYAlO_4$:Eu system under a reducing atmosphere. All the emissions spectra are intense. The most intense emission at around 622 nm is attributed to the hypersensitive transition $^5D_0 \rightarrow {}^7F_2$, indicating that the Eu^{3+} ions mainly occupy the sites without inversion symmetry. The more intense emission at 702 nm is rarely reported. This peak comes from the $^5D_0 \rightarrow {}^7F_4$ transition of Eu^{3+}. As shown in Fig. S2,† the excitation peaks are similar under the different monitoring wavelength ($\lambda_{em} = 592$, 621, 702 nm), which indicates that the emission peaks of Eu^{3+} at 592, 621, 702 nm comes from the same site of Eu^{3+}.

Fig. 3(b and f) show the emission spectra of $CaY_{0.9}Al_{1.1}O_4$:Eu and $CaY_{0.8}Al_{1.2}O_4$:Eu under the excitation of 365 nm, respectively. It is surprising to find an appearance of a broad band with the peak at 445 nm except for some sharp peaks in the range of 350–500 nm related to the 4f–4f transitions of Eu^{3+} ions. Fig. 3(e and h) show the PL spectra of $CaY_{0.9}Al_{1.1}O_4$:Eu and $CaY_{0.8}Al_{1.2}O_4$:Eu under the monitoring wavelength at 445 and

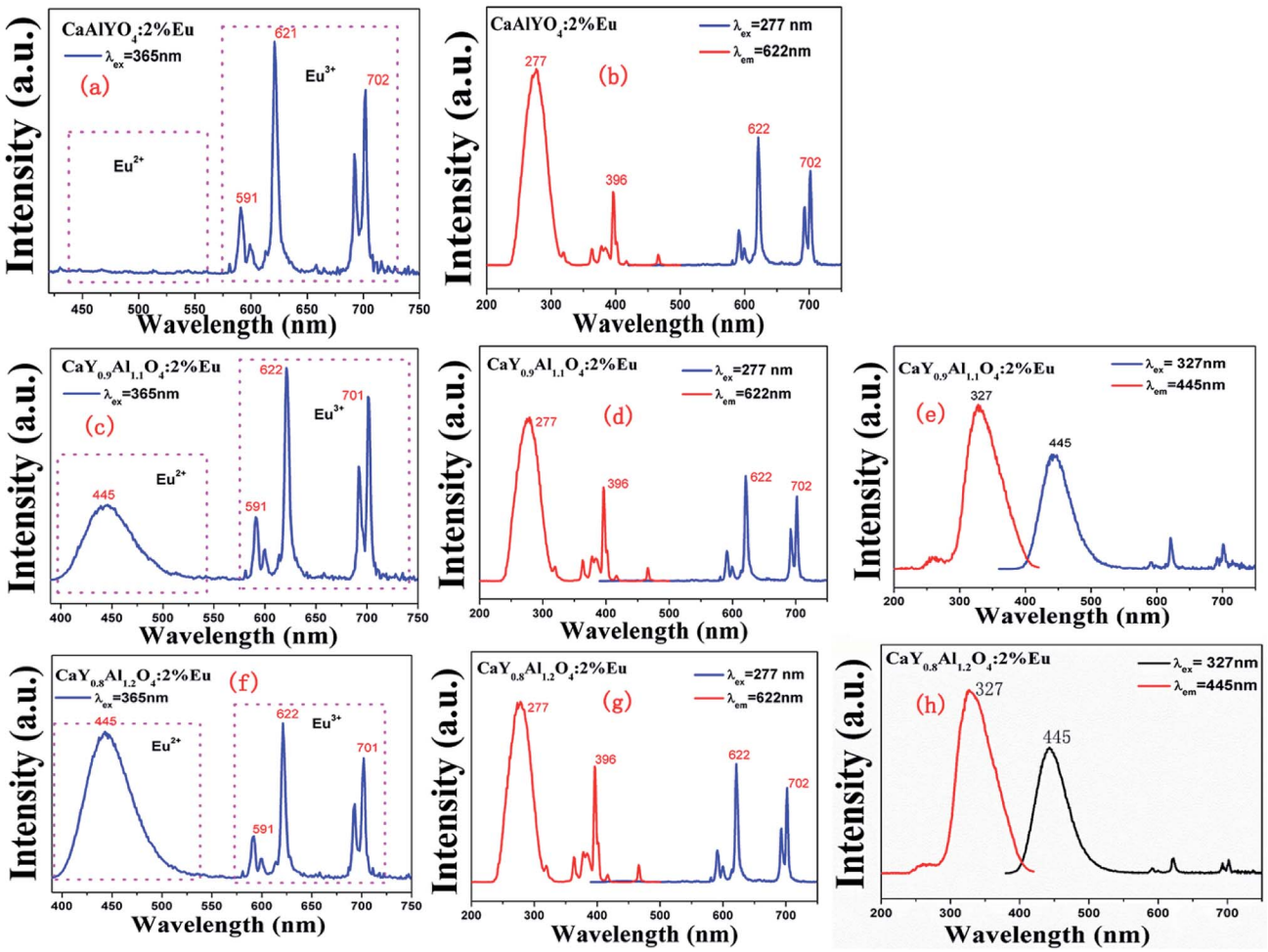

Fig. 3 (a), (c) and (f) are the emission spectra of $CaYAlO_4$:Eu, $CaY_{0.9}Al_{1.1}O_4$:Eu and $CaY_{0.8}Al_{1.2}O_4$:Eu under the excitation wavelength at 365 nm, respectively. (b), (d) and (g) are the excitation spectra under the monitoring wavelength at 622 nm and the emission spectra under the excitation wavelength at 277 nm under excitation wavelength of $CaYAlO_4$:Eu, $CaY_{0.9}Al_{1.1}O_4$:Eu and $CaY_{0.8}Al_{1.2}O_4$:Eu, respectively. (e) and (h) are the excitation spectra under the monitoring wavelength at 445 nm and the emission spectra under the excitation wavelength at 327 nm of $CaY_{0.9}Al_{1.1}O_4$:Eu and $CaY_{0.8}Al_{1.2}O_4$:Eu, respectively.

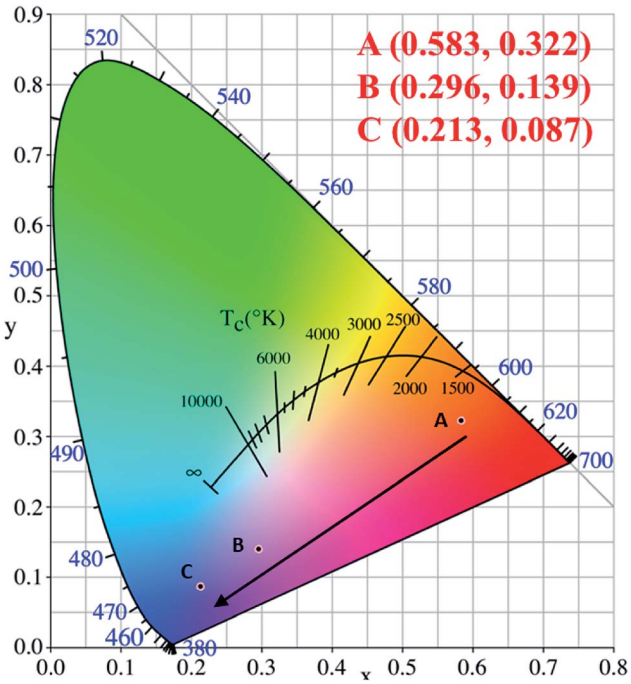

Fig. 4 The corresponding CIE chromaticity diagram for $CaY_{1-x}Al_{1+x}O_4$:2%Eu ($x = 0$, 0.1, 0.2) under the 365 nm excitation. (A) $x = 0$; (B) $x = 0.1$; (C) $x = 0.2$.

the PLE spectra under the excitation wavelength at 327. These correspond to the $4f^6 5d^1$–$4f^7$ transition of Eu^{2+}. This indicates that Eu^{3+} had been directly reduced to Eu^{2+} in $CaY_{0.9}Al_{1.1}O_4$:Eu and $CaY_{0.8}Al_{1.2}O_4$:Eu system under a reducing atmosphere. The luminescence intensity of Eu^{2+} increases with increasing x in $CaY_{1-x}Al_{1+x}O_4$:2%Eu ($x = 0$, 0.1, 0.2) system (Fig. S4†), which can be attributed to the increase of x value. These results suggest that Eu^{3+} is partially transformed to Eu^{2+} in $CaY_{1-x}Al_{1+x}O_4$:2%Eu ($x = 0$, 0.1, 0.2).

The corresponding CIE chromaticity diagram for $CaY_{1-x}Al_{1+x}O_4$:2%Eu ($x = 0$, 0.1, 0.2) has been shown in Fig. 4. The points A, B and C stand for the CIE coordinate position when $x = 0$, 0.1 and 0.2, respectively. With increasing of the Al/Y ratio in $CaY_{1-x}Al_{1+x}O_4$:2%Eu, the emission color changed from A (0.583, 0.322) red to C (0.213, 0.083) blue.

The diffuse reflectance in the UV-vis region was used to calculate the experimental band-gap value of $CaY_{1-x}Al_{1+x}O_4$:Eu^{3+}($x = 0$, 0.1, 0.2). Fig. 5 illustrates the diffuse reflectance of $CaY_{1-x}Al_{1+x}O_4$:2%Eu ($x = 0$, 0.1, 0.2). The results show that the samples begin to exhibit low reflectance below 330 nm due to the high radiation absorption. This behavior is assigned to the edge absorption, corresponding to the electronic transition from the valence band to the conduction band of $CaYAlO_4$. The matrix of yttrium aluminate and calcium shows optical transparency in the visible region between 330 and 750 nm, making it a candidate for applications in photonic devices.

In Fig. 5b–d, the $(h\nu F(R_\infty))^2$ of $CaY_{1-x}Al_{1+x}O_4$:2%Eu ($x = 0$, 0.1, 0.2) was plotted against the ($h\nu$) using the Kubelka–Munk function.[31] The following relational expression proposed by Tauc, Davis, and Mott is used:[32,33]

$$[\alpha h\nu]^n = A(h\nu - E_g) \quad (1)$$

where h is Planck's constant, ν is frequency of vibration, α is absorption coefficient, E_g is band gap, and A is proportional constant. $h\nu$ represents the energy per photon, E_g is the value of the band gap, $n = 1/2$ means a indirect allowed transition, 2 represents a direct allowed transition, 3/2 stands for a direct forbidden transition, or 3 indicates as indirect forbidden transition. Since the direct allowed transition is used in the experiment, $n = 2$ is used for these samples.

The acquired diffuse reflectance spectra of $CaY_{1-x}Al_{1+x}O_4$:2%Eu ($x = 0$, 0.1, 0.2) in Fig. 5 are converted to Kubella–Munk equation:[32,34]

$$F(R_\infty) = \frac{(1 - R_\infty)^2}{2R_\infty} \quad (2)$$

where R_∞ is the diffuse reflectance of the layer relative to the standard. Thus, the vertical axis is converted to quantity $F(R_\infty)$, which is proportional to the absorption coefficient α. The α in the Tauc equation is substituted with $F(R_\infty)$. Thus, in the actual experiment, the relational expression (1) becomes:[23,34]

$$(h\nu F(R_\infty))^2 = C(h\nu - E_g) \quad (3)$$

where C is a proportional constant. Using the Kubelka–Munk function, the was plotted against the $h\nu$. The curves that plots the value of ($h\nu - (h\nu F(R_\infty)^2)$ on the horizontal axis $h\nu$ and vertical axis $(h\nu F(R_\infty))^2$ are drawn in Fig. 5(b–d). Here, the unit for $h\nu$ is eV (electron volts), and its relationship to the wavelength λ (nm) becomes $h\nu = 1239.7/\lambda$. A red lines are drawn tangent to the point of inflection on the black curves. The values associated with the point of intersection of the lines tangent to the plotted curve inflection point with the horizontal axis ($h\nu$ axis) becomes the band gap E_g value. Their band gaps of $CaY_{1-x}Al_{1+x}O_4$:2%Eu ($x = 0$, 0.1, 0.2) are 4.10, 4.10 and 4.11 eV. The results show that a significant changing cannot be found in the band-gap edge with increasing value of x. In fact, the R. V. Perrella's[34] reported that the difference of energy band-gap between samples doped with 1 and 10 mol% of Eu^{3+} is in the order of magnitude of the phonon energy of the lattice, the Eu^{3+} substitute Y^{3+} cannot change the band gap. Here, when the x increases and cause the band gap also unchanged, so we infer that Al^{3+} also substitute the Y^{3+} site rather than Ca^{2+} site.

The decay curves of Eu^{3+} shown in Fig. 6a–c are accurately fitted using the following single-exponential equation:

$$I(t) = I_0 \exp\left(\frac{-t}{\tau}\right) \quad (4)$$

where I_t and I_0 are the intensity at time t and time zero, respectively, the τ is the lifetime. When under the excitation wavelength of 394 nm, the lifetimes of Eu^{3+} in $CaYAlO_4$:Eu, $CaY_{0.9}Al_{1.1}O_4$:Eu and $CaY_{0.8}Al_{1.2}O_4$:Eu are 1.198 ms, 1.190 ms and 1.201 ms, respectively.

The decay curves of Eu^{2+} in Fig. 6d and e are accurately fitted well to a second-order exponential decay model based on the following formula:

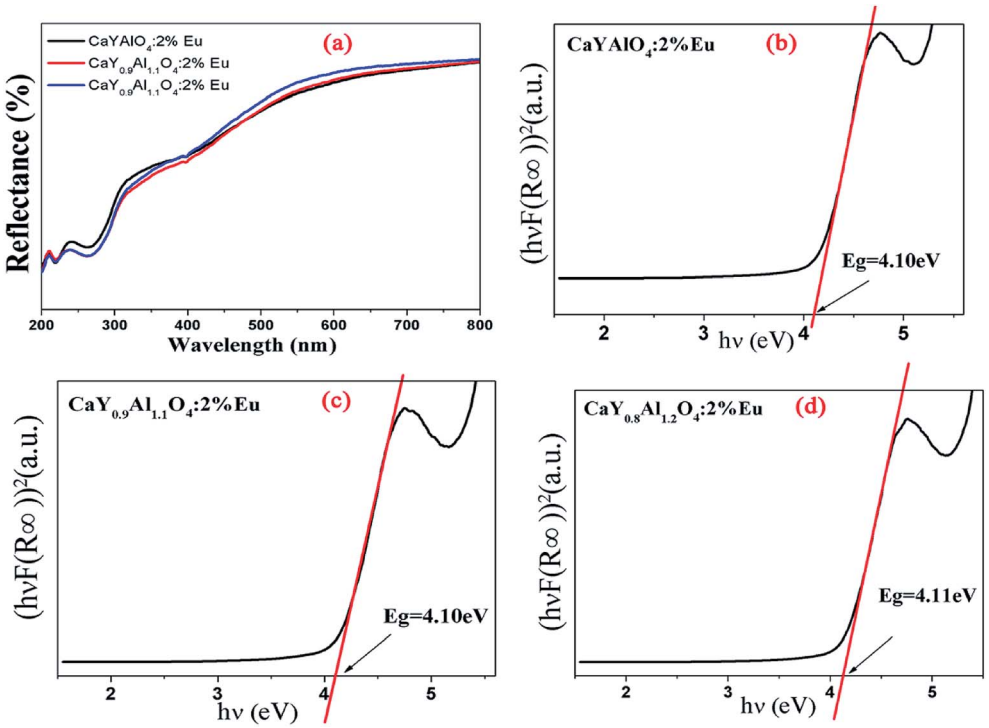

Fig. 5 (a) Diffuse reflectance of $CaY_{1-x}Al_{1+x}O_4$:2%Eu (x = 0, 0.1, 0.2). (b), (c) and (d): The $(h\nu F(R_\infty))^2$ was plotted against the ($h\nu$) using the Kubelka–Munk function.

$$I(t) = A_1 \exp\left(-\frac{t}{\tau_1}\right) + A_2 \exp\left(-\frac{t}{\tau_2}\right) \quad (5)$$

where $I(t)$ is the luminescence intensity at times t. A_1 and A_2 are fitting constants, τ_1 and τ_2 are exponential component of the decay time and t is the time, respectively. The average decay time can be described by the following formula:

$$\tau = \frac{(A_1\tau_1^2 + A\tau_2^2)}{(A_1\tau_1 + A_2\tau_2)} \quad (6)$$

According to the equation, the lifetimes of Eu^{2+} in $CaY_{0.9}Al_{1.1}O_4$:Eu and $CaY_{0.8}Al_{1.2}O_4$:Eu are calculated to be 1.07 ns and 1.14 ns, respectively.

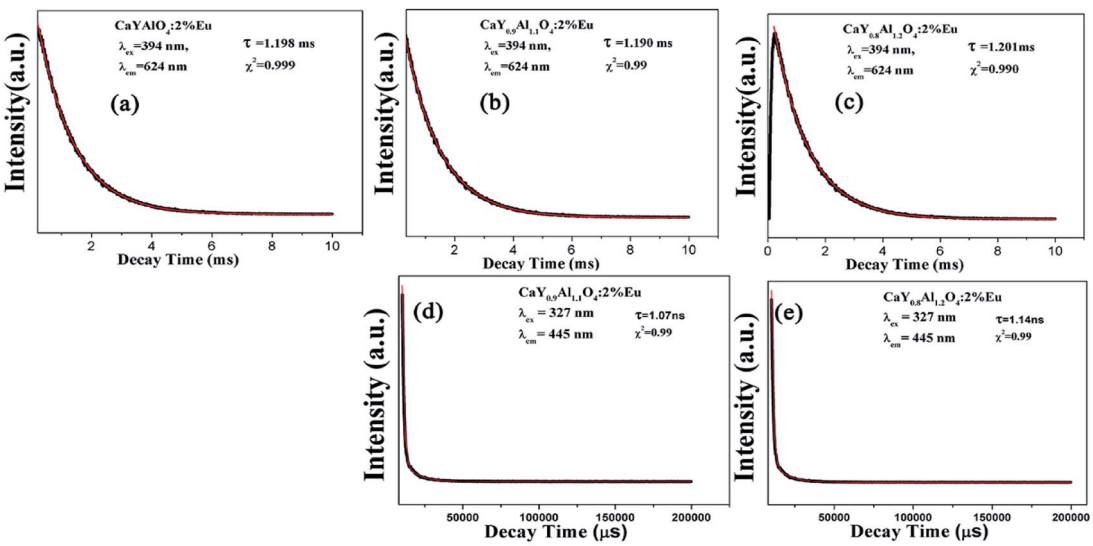

Fig. 6 (a), (b) and (c) are the decay curves of Eu^{3+} ions in $CaY_{1-x}Al_{1+x}O_4$:2%Eu (x = 0, 0.1, 0.2) (λ_{ex} = 394 nm, λ_{em} = 624 nm). The (d) and (e) are the decay curves of Eu^{2+} ions in the $CaY_{1-x}Al_{1+x}O_4$:2%Eu (x = 0.1, 0.2) sample (λ_{ex} = 327 nm, λ_{em} = 445 nm).

3.3 Bond energy method and preferential occupancy of Eu ions

The dopant occupancy in the matrix can be determined by comparing the deviation of its bond energy in different lattice location. The similar value of the deviation for its bond energy, the more stable the dopants in matrix are. Thus, to determine which site Eu^{3+} and Eu^{2+} will occupy, the bond-energy method has been used to study to the local structure Eu^{3+}/Eu^{2+} in $CaYAlO_4$ crystals. The bond energy of different dopants in $CaYAlO_4$ crystallographic frame can be estimated through the following equation:[19,21,22]

$$E_{Ca/Y/Al-O} = J \exp\left(\frac{d_0 - d_{Ca/Y/Al-O}}{0.37}\right)\left(\frac{V_{Ca/Y/Al}}{V_{Eu}}\right) \quad (7)$$

V_{Eu} is valence state of Eu (including +2 or +3), both J and d_0 are constant usually they can be found in reference. $E_{Ca/Y/Al-O}$ is mean the bond energy of Ca–O, Y–O or Al–O. In the case of pure $CaYAlO_4$ crystals without any dopant, $V_{Ca/Y/Al}/V_{Eu}$ is equal to 1. The eqn (7) can be expressed as:[19,21,22]

$$E_{Ca/Y/Al-O} = J \exp\left(\frac{d_0 - d_{Ca/Y/Al-O}}{0.37}\right) \quad (8)$$

and if is not equal to 1, then it means the valence state affects the crystal bond energy effectively.

It is assumed that the Eu^{3+}–O^{2-} bonds have the similar bond lengths as Ca/Y/Al–O bonds when the dopant substitutes Ca/Y/Al cations. In this regard, the value of various un-doped and doped $CaYAlO_4$ crystals can be evaluated. The displacement of dopants leads to a large variation of the crystal composition and bond energy, which may affect not only the crystal properties but also the crystal stability. In such a case, it is convenient to measure the variation of bond energy by the following expression when the Eu locates at Ca/Y/Al sites. Based on chemical viewpoint, the dopants preferentially occupy the sites with smaller alterations of bond energy, the sites with smaller absolute values can be expressed as below,[19,21,22]

$$\Delta E_{Eu}^{Ca/Y/Al} = |E_{Ca/Y/Al-O} - E_{Eu-O}| \quad (9)$$

Here $\Delta E_{Eu}^{Ca/Y/Al}$ is the variation of bond energy when the Eu locates at Ca/Y/Al sites. Based on chemical viewpoint, the dopants preferentially occupy the sites with smaller deviation of bond energy ($E_{Ca/Y/Al-O}$), the sites with smaller absolute values of $\Delta E_{Eu}^{Ca/Y/Al}$.

According to the bond energy method, the values of bond energy of $CaY_{1-x}Al_{1+x}O_4$:2%Eu ($x = 0.1, 0.2$) have been shown in Table 3. The order of variation of bond energy under the assumption that $Ca^{2+}/Y^{3+}/Al^{3+}$ ions are substituted by Eu^{3+} is $\Delta E_{Eu^{3+}}^{Y}$ (3.236 kcal mol^{-1}) < $\Delta E_{Eu^{3+}}^{Ca}$ (6.533 kcal mol^{-1}) ≪ $\Delta E_{Eu^{3+}}^{Al}$ (118.789 kcal mol^{-1}), which means that Eu^{3+} will preferentially replaces Y^{3+}. The calculation result is consistent with the experiment. In addition, the order of variation of bond energy Eu^{2+} substituted Y^{3+}, Ca^{2+} and Al^{3+} is $\Delta E_{Eu^{2+}}^{Y}$ (12.386 kcal mol^{-1}) ≈ $\Delta E_{Eu^{2+}}^{Ca}$ (12.633 kcal mol^{-1}) ≪ $\Delta E_{Eu^{3+}}^{Al}$ (67.149 kcal mol^{-1}), which means that the site of Ca^{2+} and Y^{3+} could be replaced by Eu^{2+} equally. Considering the valence of Eu^{2+}, we can determine that the Eu^{2+} is preferentially occupied the site of Ca^{2+}.

3.4 The $^5D_0$–$^7F_4$ emission for $CaY_{1-x}Al_{1+x}O_4$:2%Eu ($x = 0$, 0.1, 0.2)

The emission spectrum showed an unusual comparable intensity $^5D_0$–$^7F_4$ transition peak. The relative intensity of $^5D_0$–$^7F_2$ and $^5D_0$–$^7F_4$ can be stable by changing the relative proportions of Al^{3+} and Y^{3+}. To gain some insight into the nature of the luminescence behavior of Al^{3+} ions in crystal $CaYAlO_4$:2%Eu powders, the Judd–Ofelt model was applied to the determination of spontaneous emission coefficients. The intensity parameters Ω_2 and Ω_4 were determined from luminescence spectra using the method proposed by Kodaira *et al.*[28,35]

The emission intensity, $I = \hbar\omega AN$, is expressed in terms of the surface under the emission curve, where $\hbar\omega$ is the transition energy, N is the population of the emitting level ($^5D_0$) and the Einstein's coefficient of spontaneous emission can be given by[25]

$$A_{0-\lambda} = \frac{4e^2\omega^3}{3\hbar c^3}\chi\sum_{\lambda=2,4}\Omega_\lambda\left\langle {}^5D_0\|U^{(\lambda)}\|{}^7F_J\right\rangle^2 \quad (10)$$

where $\chi = n_0(n_0{}^2 + 2)^2/9$ is a Lorentz local field correction. The square reduced matrix elements are $\langle {}^5D_0\|U^{(2)}\|{}^7F_2\rangle^2 = 0.003289$; $\langle {}^5D_0\|U^{(2)}\|{}^7F_4\rangle^2 = 0.002365$ in eqn (10) and an average index of refraction equal to 1.5 was used.[36] In this case the $A_{0-\lambda}$ values are obtained by using the relation:[25,37]

$$A_{0-\lambda} = A_{0-1}\frac{S_{0-\lambda}}{S_{0-1}}\frac{\sigma_\lambda}{\sigma_1} \quad (11)$$

where $S_{0-\lambda}$ is the area under the curve related to the $^5D_0$–$^7F_\lambda$ transition obtained from the spectral data, σ_λ is the energy barycenter of the 0–λ transition and A_{0-1} is the Einstein's coefficient for the 0–1 magnetic dipole transition. The A_{0-1} value is estimated to be around of 50 s^{-1}.

The lifetime (τ), non-radiative (A_{nrad}) and radiative (A_{rad}) rates are related through the following equation:[35]

$$A_{tot} = \frac{1}{\tau} = A_{rad} + A_{nrad} \quad (12)$$

where the radiative (A_{rad}) rates was obtained by summing over the radiative rates A_{0-J} for each $^5D_0$–^7F_J transitions. It can be given by:[35]

$$A_{rad} = \sum_J A_{0-J} \quad (13)$$

The emission quantum efficiency of the emitting $^5D_0$ level is given by:[35]

$$\eta = \frac{A_{rad}}{A_{rad} + A_{nrad}} \quad (14)$$

The values of the Ω_2 and Ω_4 parameters as well as other quantities derived from analysis of the luminescence spectra of Al^{3+} replace the Y^{3+} in $CaYAlO_4$ are given in Table 4.

Table 4 shows intensity parameters Ω_2 and Ω_4. Ω_λ is the emission intensity parameters; Ω_2 is the emission intensity parameter of $^5D_0$–$^7F_2$. Ω_4 means the emission intensity parameter of $^5D_0$–$^7F_4$. Here, the Ω_2 intensity parament values are higher than Ω_4 for $CaY_{1-x}Al_{1+x}O_4$:2%Eu ($x = 0$, 0.1, 0.2). The

Table 3 The bond parameters of the central atom and values of bond energy when Eu^{3+} locates at Ca, Y, and Al sites in $CaYAlO_4$. All of the bond energy unit are kcal mol^{-1}

Central atom	Coordination atom	Count	d (Å)	E_{M-O}	$E_{Eu^{3+}}$	$E_{Eu^{2+}}$	$\Delta E^{M}_{Eu^{3+}}$	$\Delta E^{M}_{Eu^{2+}}$
Ca1	O2	1×	2.3013	51.291	39.457	28.407	6.533	12.633
	O1	4×	2.5152	28.772	22.133	15.935		
	O2	4×	2.6125	22.119	17.015	12.250		
Al1	O1	4×	1.8375	73.757	207.306	149.253	118.784	67.149
	O2	2×	1.9866	49.294	138.549	99.750		
Y1	O2	1×	2.3013	65.045	59.186	42.611	3.236	12.385
	O1	4×	2.5152	36.488	33.200	23.903		
	O2	4×	2.6125	28.050	25.523	18.376		

Table 4 Decay rates of radiative (A_{rad}), nonradiative (A_{nrad}), and total (A_{tot}) processes of $^5D_0$–^7F_J transitions, luminescence lifetime (τ), intensity parameters (Ω_2, Ω_4), quantum efficiencies (η) and actual quantum efficiency (η_a) of $CaY_{1-x}Al_{1+x}O_4$:2%Eu

Samples	A_{rad}	A_{nrad}	A_{tot}	τ	Ω_2	Ω_4	η	η_a
$CaYAlO_4$	409	427	836	1.198	4.12	2.97	0.489	47.69%
$CaY_{0.9}Al_{1.1}O_4$	406	434	840	1.190	3.99	3.09	0.483	50.42%
$CaY_{0.8}Al_{1.2}O_4$	403	429	832	1.201	3.91	3.10	0.484	55.43%

Ω_2 parameter depends rather on the lower rank components of crystal field and dynamic coupling interactions, while the Ω_4 parament depend rather on the corresponding higher components. It suggests that site symmetry occupied by Eu^{3+} ions does not have a character of centrosymmetric chemistry environment considering that the $^5D_0$–$^7F_2$ transitions is formally forbidden due to the electric dipole selection rule. Meanwhile, it has been commented in literature that the luminescence spectra of compounds with D_{4d} (see Fig. 1(c)) symmetry are often dominated by the $^5D_0$–$^7F_4$ transition of Eu^{3+} because of the absence of central symmetry. An undistorted square antiprism has D_{4d} symmetry, so a site with symmetry lowed than D_{4d} but the coordination polyhedron close to a square antiprism, is expected to have an intense $^5D_0$–$^7F_4$ transition, In $CaY_{1-x}Al_{1+x}O_4$:2%Eu, Eu^{3+} is nine-fold coordinated, this coordination polyhedron can be regarded as close to mono-capped square-anti-prism. As a result, in this compound the $^5D_0$–$^7F_4$ transition is less intense than the $^5D_0$–$^7F_2$ transition but much more intense than $^5D_0$–$^7F_1$ magnetic dipole transition. The same remarks have also been for $LaBO_3$:Eu^{3+}, $[Eu(DOTA)(H_2O)]^-$ and $Sr_{0.99}La_{1.01}Zn_{0.99}O_{3.495}$:$Eu^{3+}$. In addition, the values of Ω_4/Ω_2 is 0.72, 0.77, 0.79 for $CaY_{1-x}Al_{1+x}O_4$:2%Eu ($x = 0$, 0.1, 0.2) respectively, which indicated the $^5D_0$–$^7F_4$ emission can be enhanced by properly adjusting the Al/Y ratio, at the same time it does not change the quantum efficiency (η). The quantum efficiency (η_a) measured by the integrating sphere is nearly the result by calculation.

4. Conclusions

A series of $CaY_{1-x}Al_{1+x}O_4$:2%Eu^{3+} ($x = 0$, 0.1, 0.2, 0.3) phosphors have been identified. The powder XRD patterns and Rietveld refinement reveal that $CaY_{1-x}Al_{1+x}O_4$:2%Eu^{3+} have a tetragonal crystal structure with the space group *I*4/*mmm* (No. 139). The photoluminescence property of the $CaY_{1-x}Al_{1+x}O_4$:2%Eu ($x = 0$, 0.1, 0.2) phosphors exhibit both blue emission of Eu^{2+} ($4f^65d^1$–$4f^7$) and red-orange emission of Eu^{3+} ($^5D_0$–$^7F_{1,2,3,4}$) under UV light excitation, which showed that $Eu^{3+/2+}$ co-doping system was obtained by adjusting Al/Y ratio. Eu^{3+} ions can be reduced to Eu^{2+} ions when Al/Y ratio was changed. Calculated by the bond-energy theory found that Eu^{3+} takes priority over the Y^{3+} site, in addition, the site of Ca^{2+} and Y^{3+} all can be occupied by Eu^{2+}. Considering the valence of Eu^{2+}, it can determine that the Eu^{2+} is preferentially occupied the site of Ca^{2+}. The Judd–Ofelt model was applied to the determination of spontaneous emission coefficients. The intensity parameters Ω_2 and Ω_4 were determined from luminescence spectra.

Conflicts of interest

There are no conflicts to declare.

Acknowledgements

This work is financially supported by the National Natural Science Foundations of China (Grant no. 21301053 and 21571165) and Hubei Natural Science Foundations from Science and Technology Department of Hubei Province (2018CFB517). This research was supported by the Basic Science Research Program though the National Research Foundation of Korea (NRF) funded by the Ministry of Science, ICT and Future Planning (No. 2018R1A2B6005179). "$Eu^{3+/2+}$ co-doping system induced by adjusting Al/Y ratio in $CaY_{1-x}Al_{1+x}O_4$:2%Eu: preparation, bond energy, site preferential and $^5D_0$–$^7F_4$ transition intensity" is supplied by the Functional Phosphor Bank at Pukyong National University.

Notes and references

1 S. Liu, G. Zhao, H. Ying, J. Wang and G. Han, *Opt. Mater.*, 2008, **31**, 47–50.
2 T. Selvalakshmi, S. Sellaiyan, A. Uedono and A. Chandra Bose, *Mater. Chem. Phys.*, 2015, **166**, 73–81.
3 K. Biswas, A. D. Sontakke, R. Sen and K. Annapurna, *J. Fluoresc.*, 2012, **22**, 745–752.

4 L. Yang, Y. Wan, Y. Huang, X. Wang, H. Cheng and H. J. Seo, *Mater. Lett.*, 2016, **172**, 23–26.
5 B. Wiendlocha, S. P. Kim, Y. Lee, B. He, G. Lehr, M. G. Kanatzidis, D. T. Morelli and J. P. Heremans, *Phys. Chem. Chem. Phys.*, 2017, **19**, 9606–9616.
6 P. L. Roeder, D. MacArthur, X. P. Ma, G. R. Palmer and A. N. Mariano, *Am. Mineral.*, 1987, **72**, 801–811.
7 Y. Su, L. Li and G. Li, *Chem. Mater.*, 2008, **20**, 6060–6067.
8 H. You and C. Shi, *Chin. Sci. Bull.*, 1996, **41**, 123–126.
9 J.-G. Kang, J.-S. Jung, J.-P. Hong, S.-J. Won, Y. Sohn and C. K. Rhee, *J. Phys.: Condens. Matter*, 2001, **13**, 2835–2843.
10 Z. Pei, Q. Zeng and Q. Su, *J. Phys. Chem. Solids*, 1999, **61**, 9–12.
11 J. S. Zhong, H. B. Gao, Y. J. Yuan, L. F. Chen, D. Q. Chen and Z. G. Ji, *J. Alloys Compd.*, 2018, **735**, 2303–2310.
12 Z. Jiang, X. Yu, J. Gou, L. Duan, X. Su, G. Fan and Y. Duan, *J. Mater. Sci.: Mater. Electron.*, 2017, **28**, 3630–3636.
13 H. Chen, X. Huang and W. Huang, *Chin. J. Phys.*, 2016, **54**, 931–939.
14 K. Li, H. Lian, M. Shang and J. Lin, *Dalton Trans.*, 2015, **44**, 20542–20550.
15 Y. Wang, J. Ding, Y. Li, L. Yang, X. Ding and Y. Wang, *RSC Adv.*, 2016, **6**, 42618–42626.
16 Y. Zhang, X. Li, K. Li, H. Lian, M. Shang and J. Lin, *ACS Appl. Mater. Interfaces*, 2015, **7**, 2715–2725.
17 K. Kumar, A. K. Singh and S. B. Rai, *Spectrochim. Acta, Part A*, 2013, **102**, 212–218.
18 Y. Zhang, J. Chen, C. Xu, Y. Li and H. J. Seo, *Phys. B*, 2015, **472**, 6–10.
19 Y. He and D. Xue, *J. Phys. Chem. C*, 2007, **111**, 13238–13243.
20 L. Li, W. Wang, Y. Pan, Y. Zhu, X. Liu, H. M. Noh, B. K. Moon, B. C. Choi and J. H. Jeong, *RSC Adv.*, 2018, **8**, 1191–1202.
21 L. Li, J. Cao, B. Viana, S. Xu and M. Peng, *Inorg. Chem.*, 2017, **56**, 6499–6506.
22 L. Li, Y. Pan, W. Wang, Y. Zhu, W. Zhang, H. Xu, L. Zhou and X. Liu, *J. Alloys Compd.*, 2018, **731**, 496–503.
23 R. Shi, B. Li, C. Liu and H. Liang, *J. Phys. Chem. C*, 2016, **120**, 19365–19374.
24 Z. Babakhanova, M. Aripova and E. Bernardo, *Glass Ceram.*, 2016, **73**, 124–127.
25 R. A. Sa Ferreira, S. S. Nobre, C. M. Granadeiro, H. I. S. Nogueira, L. D. Carlos and O. L. Malta, *J. Lumin.*, 2006, **121**, 561–567.
26 M. Xie, Y. Li and R. Li, *J. Lumin.*, 2013, **136**, 303–306.
27 G. K. Behrh, R. Gautier, C. Latouche, S. Jobic and H. Serier-Brault, *Inorg. Chem.*, 2016, **55**, 9144–9146.
28 A. Strzep, A. Watras, K. Zawisza, P. Boutinaud and R. J. Wiglusz, *Inorg. Chem.*, 2017, **56**, 10914–10925.
29 D. Geng, G. Li, M. Shang, C. Peng, Y. Zhang, Z. Cheng and J. Lin, *Dalton Trans.*, 2012, **41**, 3078–3086.
30 S. Lv, Y. Wang, Z. Zhu, Z. You, J. Li, S. Gao, H. Wang and C. Tu, *Appl. Phys. B: Lasers Opt.*, 2014, **116**, 83–89.
31 J. Chen, W. Zhao, J. Wang and N. Wang, *J. Mater. Sci.: Mater. Electron.*, 2016, **27**, 237–244.
32 Y. Su, L. Peng, C. Du and X. Wang, *J. Phys. Chem. C*, 2012, **116**, 15–21.
33 Y. Su, L. Peng, J. Guo, S. Huang, L. Lv and X. Wang, *J. Phys. Chem. C*, 2014, **118**, 10728–10739.
34 R. V. Perrella, C. S. Nascimento Jr, M. S. Goes, E. Pecoraro, M. A. Schiavon, C. O. Paiva-Santos, H. Lima, M. A. Couto dos Santos, S. J. L. Ribeiro and J. L. Ferrari, *Opt. Mater.*, 2016, **57**, 45–55.
35 C. A. Kodaira, H. F. Brito, O. L. Malta and O. A. Serra, *J. Lumin.*, 2003, **101**, 11–21.
36 R. D. L. Gaspar, E. M. Rodrigues, I. O. Mazali and F. A. Sigoli, *RSC Adv.*, 2013, **3**, 2794.
37 Q. Zhang, X. Wang, X. Ding and Y. Wang, *Inorg. Chem.*, 2017, **56**, 6990–6998.